Overcoming the variability of fingertip friction with surface-haptics force-feedback

Nicolas Huloux[1], Jocelyn Monnoyer[1,2],
Marc Boyron[1], Michaël Wiertlewski[1]

[1] Aix-Marseille Université, CNRS, ISM UMR 7287, 13009, Marseille, France
[2] PSA Peugeot Citroën
`firstname.lastname@univ-amu.fr`

Abstract. Touch screens have permeated our lives as the human-machine interface of choice, and as a consequence, producing vivid tactile sensations on these flat panels is the subject of active research. One of the leading methods uses ultrasonic vibration to controllably reduce the friction experienced by a finger touching a glass plate. Typically, devices modulate the amplitude of the vibration in order to control the frictional force that the finger experiences without monitoring the actual output. However, because friction is a complex physical process, the open-loop transfer function is not stationary and varies with a wide range of external parameter such as velocity of exploration or moisture. We present a new interface that incorporates a force sensor able to pick up subtle fluctuations of the frictional force on a wide frequency bandwidth that includes static forces. This force sensor is the basis for real time control of the frictional force of the finger, which reduces significantly the inherent variability of ultrasonic friction modulation while maintaining a noise level below human perception thresholds. The interface is able to render of precise and sharp frictional patterns directly on the user's fingertip.

Keywords: Surface Haptic, Force feedback, Closed loop control.

1 Introduction

Surface-haptic promises to restore the tangibility of virtual interfaces while interacting with flat and featureless touchscreens. Virtual bumps, texture, clicks and scrolling effects produce sensations that guides the users' motion and offer feedback on their action. To date, one of the most promising ways to produce rich sensations is to modulate the friction between the finger and the plate either via electrostatic adhesion [1] or via ultrasonic squeeze-film levitation [2, 3]. The main advantage over vibrotactile stimulation is that it produces stimuli that not only include transient events –i.e. texture, impacts or vibrations– but affects continuous forces. Slowly modulating the force enable the production of tactile illusions of shape and large reliefs such as bumps and holes, in line with robotic force feedback devices [4, 5].

In spite its advantages, friction modulation produce signals that are distorted and attenuated [6, 7]. The main factor of the signal variance is that the frictional behavior of a finger sliding onto a glass plate is complex. The angle of the finger, the pressing force, and the moisture of the skin affect the friction force[8]. Worst of all, even if the exploration condition are accounted for, sweating and subsequent softening of the stratum corneum induce large variation of friction over time [9].

In addition to relying on friction to produce forces to the fingertip, the two leading technologies have their intrinsic drawbacks. Electro-adhesion, while having a large functional bandwidth and potentially strong forces, exhibits non-linearities that distord the signal [1]. Squeeze-film levitation using ultrasonic standing waves is able to modulate the friction force on a larger dynamic range, but suffers from a poor frequency response [10] and large static non-linearity [11]. Combining both effects to increase the dynamic range of possible signal have been proposed [12, 13] but does not solve the inherent variability of the friction force modulation.

Feedforward compensation filters can counteract the attenuation inherent to ultrasonic friction modulation and provide a fast and clear signal to the user. The faster dynamic is achieved by temporally overdriving the actuators to rapidly reach a given friction force [14]. Distortions due to static non-linearity can be corrected by a look-up table [15]. While these feedforward model-based approaches improve over the open-loop performance, the inherent variability prevents to precisely regulate a given force. Ben Messaoud et al. proposed to tackle this drawbacks by using a real-time measurement of the friction force that informs a closed-loop feedback control to reject unknown disturbances [16]. The control uses a robust sliding mode strategy to remove static error and improve the dynamic response.

However, like any closed-loop control system, noise from the force sensor was re-injected into the actuators, which resulted in a noisy rendering. In order to circumvent the limitation of this approach, we developed a custom built capacitive-sensor that can resolve the force with a dynamic range higher than 1:50,000. Using this sensor in a force feedback scheme, results in a low noise, yet fast and accurate control of the friction force using a state-of-the-art proportional-integral controller.

2   Simulations

2.1   Linearized dynamic model of ultrasonic friction modulation

In order to capture the stochastic nature of ultrasonic friction modulation and to set up the most appropriate controller, the relationship between the amplitude set on the plate and the frictional force that is actually produced needs to be modeled. Measurements of a large dataset (n = 26) of amplitude and force values relationship when participants explored a plate excited by a 1Hz amplitude modulated 2.5μm and 30kHz ultrasonic carrier at various exploration

speed, forces and finger posture is presented in Fig. 1a. While the individual trials might exhibit a clear negative correlation between vibration amplitude and friction force, the relationship from trial-to-trial is not consistent. To capture this behavior, the non-linear Gaussian model described in [11] was extended by adding an unknown perturbation d that is bounded so to avoid negative values of the friction force. The modified friction force model is:

$$f = f_0 \exp(-a^2\tau) + d = g(a) + d \tag{1}$$

where $f_0 = 0.8$ N is the nominal friction force, a is the vibration amplitude, $\tau = 0.38$ μm^{-2} is the susceptibility to ultrasonic levitation. The deterministic behavior is referred by the function $g(a)$ and we set d to be a 1 Hz sine wave of 0.8 N amplitude and 0.4 N offset.
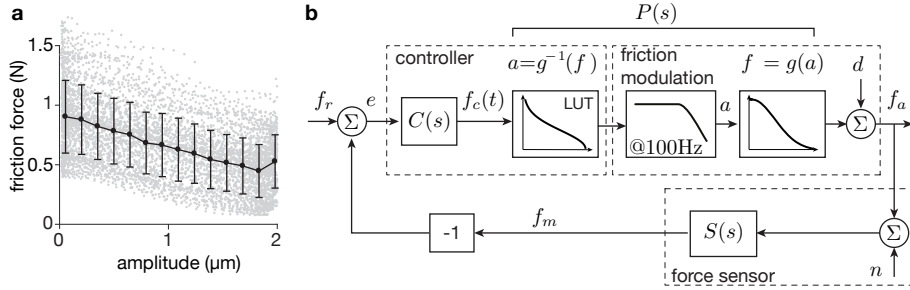

Fig. 1: **a** Friction force and amplitude data points for 26 sliding trials are shown in gray. Average and standard deviation are reported in black. **b**. Block diagram of the control scheme.

2.2 Control strategy

The block diagram of the control strategy implemented in this article is found Fig 1b. The friction modulation process, that takes amplitude as input and outputs a friction force, is modeled by a linear time-invariant function that acts a first order low pass filter with a cutoff at 100 Hz to match the attenuation reported in [10]. The filter is followed by the non-linear relationship described by equation 1 to complete the model of the friction modulation process.

A lookup table is implemented in the controller to compensate the non-linearity of ultrasonic friction modulation captured by equation 1. The lookup table and the friction modulation process can be lumped into a single linear time-invariant transfer function called $P(s)$ associated to a saturation function where the amplitude of the ultrasonic wave is bounded between 0 and 2.5 μm. Therefore, the controller $C(s)$ has to compensate for the corrected process $P(s)$, which acts as a first-order low-pass filter, and for an unknown disturbance d, which evolves at a slow pace.

A force sensor measures the friction force that is applied to the finger along with some undesired noise n. It typically follows a zero-mean random Gaussian process. The dynamic of the sensor is modeled by the transfer function $S(s)$, which for ease of simulation, is considered to be a low-pass filter with a cutoff frequency of 1 kHz. The measured force f_m is then subtracted to the set-point force f_r to compute the error e, which is subsequently fed to the controller.

2.3   Precision and accuracy trade-off

The ideal control scheme has a fast and effective disturbance rejection without adding any noise to the output of the system. In practice the two objectives leads to opposite constrains on the controller. In the current implementation, we chose a proportional-integral controller such that $C(s) = K_p + K_i/s$. A higher set of gain K_p and K_i allows for a fast convergence, but results in an amplification of the noise introduced by the sensor. This noise is detrimental to the user's tactile experience as it adds fluctuations that are not part of the original signal. This trade-off between the convergence to a precise value (accuracy) and the noise injected (precision) into the closed loop has to be evaluated and will lead to a constrain of the maximum noise that the sensor can generate.

From the block diagram described in Fig. 1, and considering only the linear behavior, we can derive the expression of the force perceived by the finger in the Laplace domain as:

$$f_a = d\,\frac{1}{1+G} + f_r\,\frac{CP}{1+G} - n\,\frac{G}{1+G} \tag{2}$$

where $G(s) = C(s)P(s)S(s)$. To study the effect of the noise n on the variance of the friction force σ_f^2, we can consider that the variance of the setpoint and the disturbance are null in steady-state. Therefore error propagation analysis leads to the following relationship:

$$\sigma_f^2 = \left|\frac{G}{1+G}\right|^2 \sigma_n^2 \tag{3}$$

This relationship highlights that the noise perceived by the user, σ_f^2 is affected by the gain of the closed-loop control. A lower gain attenuates the noise of the sensors. Conversely, since the disturbance is affected by the sensitivity function $\frac{1}{1+G}$, which favors high gains, a trade-off has to be found.

Fig 2a shows the results of a set of simulations, where the controller parameters K_p and K_i was varied and the fidelity of the control is measured. The fidelity of the system is captured by the goodness-of-fit R^2 between the input-output relationship of the simulation compared to an ideal transfer function for which $f_a = f_r$. Both the disturbance rejection and the noise attenuation have a positive impact on the fidelity. In this simulation, the setpoint signal was a logarithmically swept-sinusoid from 1 Hz to 100 Hz of 1.2 N amplitude, the disturbance was a 1 Hz sine wave of 0.4 N amplitude and the noise was a white Gaussian noise with an amplitude of 10^{-5} N. The graph Fig 2a reveals that proportional
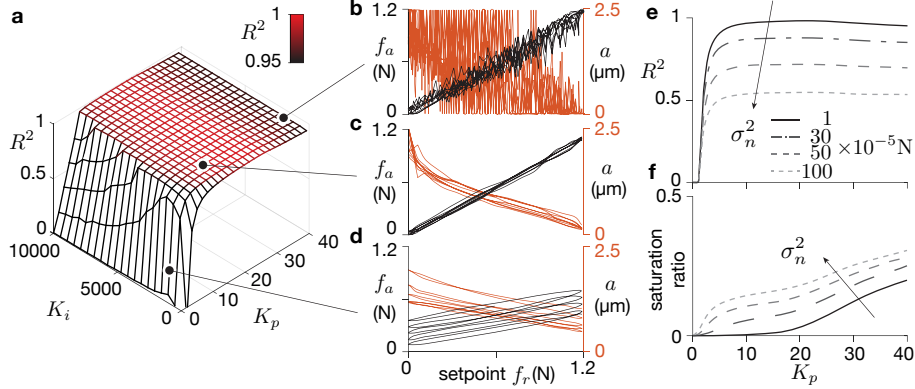
Fig. 2: **a**. The fidelity of the control captured by the R^2 metric when comparing with $f_a = f_r$, for a set of K_i and K_p coefficient. **b**. $K_i = 2$ and $K_p = 40$. Over-corrected signal leads to noise **c**.$K_i = 2$ and $K_p = 10$. The right balance between a high gain and fast convergence. **d**. $K_i = 2$ and $K_p = 1$. Low gain leads to unsatisfactory disturbance rejection. **e**. Effect of a higher sensor noise on the precision of the control. **f**. Higher noise leads to significant saturation of the controller.

gains K_p comprised between 5 and 20 offer a good disturbance rejection while avoiding to feedback significant noise. The integral term K_i is responsible for rejection of the static error but as long as it is above a value of 2 its tuning has moderate influence. The inspection of the input-output relationship for three different proportional gains $K_p = [40, 10, 1]$ is showed Fig 2b,c and d respectively. A high gain as in Fig 2b, results in noisy and saturated command, whereas a low gain as in Fig 2d results in a low precision controller. The optimum is found for value of $K_p = 10$ and $K_i = 2$, see Fig 2c.

The influence of the noise on the fidelity and the saturation of the actuation is shown in Fig.2e,f. The saturation index is calculated from the ratio of the number of datapoints that have a saturated input to the total number of data points. Noise level higher than 10^{-4} N of the force sensor will decrease significantly the precision and increase the likelihood of saturating the output. For those reasons, we chose a proportional gain of $K_p = 10$.

The simulation shows that the controller effectiveness depends on the noise added by the sensor and low noise value lead to a sharp and untainted tactile stimulation. Estimates put the lowest force perceivable by the human somatosensory system in the range of 5.10^{-4} N [14]. A sensor with a noise level of 5.10^{-5} N produces an output noise that remains subliminal.

3   Friction force sensor design

The simulation shows that the force sensor is the centerpiece of the control strategy and proper care in the choice of technology and design has to be made to achieve high-fidelity of the tactile rendering on surface-haptic devices.

3.1   Performance requirements and technology choice

The simulation shows that the noise of the sensor must be lower than 5.10^{-5} N, to make sure that the force perceived by the user remains untainted by the noise, while being able to resolve forces as high as 2.5 N. These requirements lead to a dynamic range figure of 1:50,000 or about 95 dB. Stiffness and frequency bandwidth are also crucial since they directly affect the sensor's response through the transfer function $S(s)$. A softer sensor might have a high signal to noise ratio, but at the expense of a low frequency bandwidth. The glass plate typically weighs on the order of $m_p = 400$ g and the sensor first resonance frequency is prescribed by $f_0 = 1/2\pi\sqrt{k/m_p} = 250$ Hz for a sensor stiffness of 1 N.µm. It means that to resolve 2 N, the sensor is displaced by 2µm. Since force sensors are based on the measure of the displacement of a known elastic structure, the underlying displacement sensor should have a noise floor of 0.5 pm.

The sensitivity figure excludes metal and semiconductor strain-gauge sensors which typically have signal-to-noise ratio in the order of 1:1,000 on rigid load-cells. Piezoelectric sensors, while having an exceptional signal-to-noise ratio and high-stiffness, are not suited for closed-loop feedback because of their low-frequency drift that would require frequent reset of the control loop. All these constraints are within the range of capacitive sensors which can achieve a dynamic range within the requirement while remaining impervious to drift [17].
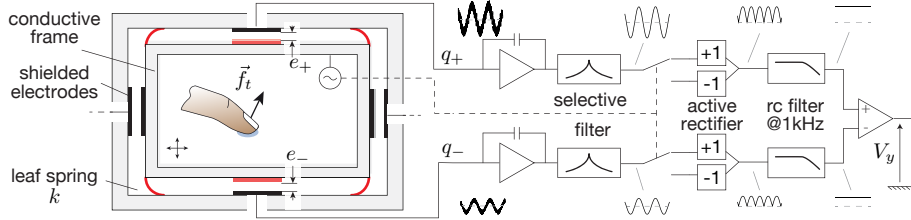

Fig. 3: Mechanical and electrical schematics of the capacitive force sensor, illustrated on one axis

3.2   Implementation

The capacitive force sensor is built around the architecture illustrated in Fig. 3. The ultrasonic plate is fixed to a frame that is suspended by four curved leaf

springs grounded to the rest of the device that deforms when the finger applies a frictional force. The motion of the plate is captured by four non-contact sensors that each measure the distance of each edge of the suspended frame to the grounded frame. The measure is differential along each dimension, with one sensor seeing a reduction in the gap, while the one on the opposite side sees an increase. This differential amplification counteracts thermal effects and unwanted electromagnetic perturbations. Each sensor is composed of one active electrode, shielded by another passive electrode. The inner frame, which is conductive, is excited by a 120 kHz sinusoidal excitation V, which polarizes the sensing electrode of the sensor. Charges $q_\pm$ that are proportional to the voltage V and inversely proportional to the distance $e_\pm$ such that $q_\pm = V \epsilon_0 A / e_\pm$, where ϵ_0 is the permittivity of air and A is the active area of the sensors.

The capacitive measurement circuit is adapted from the low-noise topology described in [17]. The charges from the sensing electrodes are transformed into a voltage via a charge amplifier and the signal is then passed through a selective filter with fundamental frequency matching the excitation or 120 kHz. After the filter, almost all artifacts of the signal are removed. At that stage, the envelope of the signal, which is related to the distance between the electrode and the outer frame, is recovered using synchronous demodulation, which includes a low pass filter with 1 kHz cutoff. The last operation takes the difference between the signal coming from two electrodes to recover the signed voltage V_s that reflects the displacement of the inner frame and therefore the force that is applied by the fingertip.

3.3   Sensor characterization

The sensor has been calibrated in quasi-static condition using a set of standard weights that applied to the frame a known gravitational force via a string and pulley system. The results can be found Fig. 4a and the linear regression shows a goodness of fit of $R^2 = 0.95$. The frequency bandwidth measurement has been made using an impact hammer. The signal was then normalized and converted to the maximum sensing value. The frequency response shows a first resonance at 145 Hz, owing to the large glass plate. The noise of the sensor was studied using a 10s sample without any external perturbation and show a floor at 5.10^{-5} N in the low frequency and an attenuation above 300 Hz, due to a series first order filter. The frequency response and noise spectrum are shown Fig. 4b. The dynamic range of the sensor before its first resonance is 1:50,000 or about 93dB.

4   Friction force feedback

4.1   Hardware

A picture of the final device is shown in Fig 4c. A glass plate of dimension $255 \times 140 \times 3$ mm^3 vibrating at 46 kHz in a 16×0 mode, provided the friction modulation. Four piezoelectric actuators are bounded to the plate and provide
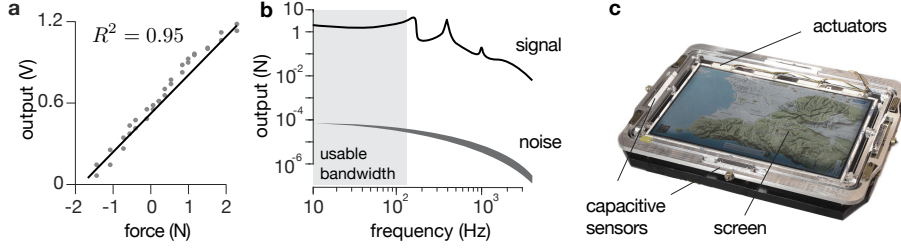
Fig. 4: **a**. Linearity of the sensor **b** Frequency spectrum of the noise and impulse response.**c** Picture of the device

a maximum displacement of 2.5 µm. It is clamped to the inner frame at the end of 3 nodal lines on each side. The outer and inner frame as well as the curved leaf spring are milled out of a single block of 2024-grade aluminum alloy.

In addition to the lateral force sensor, the system is equipped with a position sensor based on [14] and 4 normal force sensors at each corner to measure the user's finger position and normal force and be able to apply a large set of effects. The real-time control is ensured by a low-latency 5 kHz timer implemented on a micro-controller (Teensy 3.1, PRJC, Portland, OR, USA). Every 200 ms the sensors are acquired, the PI control as well as the look-up table are computed and the amplitude of the ultrasonic carrier is modulated. The amplitude modulated ultrasonic carrier is then filtered with a 10 to 50 kHz bandpass filter and amplified before being sent to the piezoelectric actuators. The controller parameters were set to $K_p = 10$ and $K_i = 2$.

4.2   Closed-loop performance

Comparison of the open-loop and closed-loop operation of the friction modulation, was done using a commanded force f_r that followed a 1 Hz sine wave between 0.3 and 0.9 N, which corresponds to a range of reliably achievable forces. This friction range has been done using three 1 Hz sine of 0.1 N amplitude with a mean of [0.4 0.6 0.8] N as setpoint to minimize the variation of friction force. The first author slid along the interface at 20mm.s^{-1}, 5 times for each force signal and recorded of 50 periods of range. Fig 5a shows that the open-loop response matches poorly the commanded force with a linear regression reveals a goodness of fit of $R^2 = 0.22$. The closed loop condition achieves a satisfactory tracking of the setpoint with linear regression leading to a goodness of fit $R^2 = 0.98$. Low friction values are causing most of the errors, in part because the large amplitude needed were not achievable by the current ultrasonic plate.

Step responses are shown in Fig. 5b. The frictional force is tracked with a time response of 37 ± 20 ms (SD) for a falling friction step and of 32 ± 16 ms for a rising friction step, in both cases for exploration speed of approximately 20 mm.s^{-1}. This figure can be improved with larger gains of the closed loop, at the expense of higher noise. The traces show that the steady state friction is not
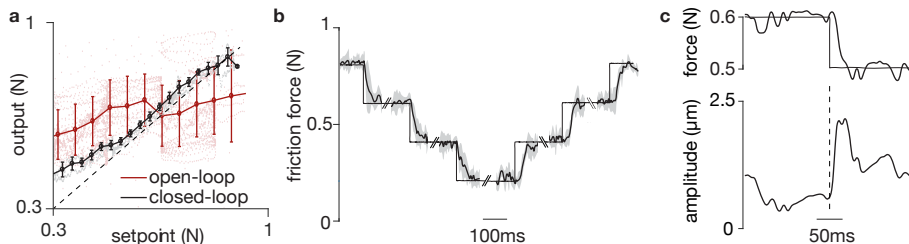
Fig. 5: Friction force feedback control. **a**. The closed loop limits the variability and compensate for the static non-linearity **b** The system response to successive unit steps shows a response time of around 30ms. **c** During a unit step, the commanded amplitude of the ultrasonic waves overshoots.

as a noise-free as one can expect from signal to noise ratio of the sensor. It seems that the additional fluctuations are due to the variability of friction and tremors of the user. Fig. 5c offers a close up view of the control strategy on a single step. In order to achieve fast response, the controller overshoots the amplitude value and then converges back to a lower steady-state value to stabilize the output.

5   Discussion

The disturbance rejection of the closed-loop force feedback is on par with the results from [16] which uses strain gauge sensor and a sliding mode controller. The steady state friction is maintained within 20 mN of the set point which is a substantial improvement of the 0.25 N variation seen when ultrasonic friction modulation is operating in open-loop.

The custom-built force sensor has a noise floor that falls below 10^{-4} N, and the gain of the controller is set to limit the noise fed back to the actuator which results in sharp tactile stimulus which is sharp and clean of artifacts. Yet the traces from Fig 5b show that the actual friction force experiences fluctuations in the order of 20 mN. These fluctuations are also present in open loop control [10] and in closed loop control that uses strain-gauge load cells [16]. The remaining fluctuations are probably the consequence of physiological and frictional noise [18], that the feedback system struggles to cancel. A frequency synthesis of the control that takes into account the friction noise could potentially lead to higher order controller that are able to cancel these fluctuations.

It is worth to note that the simulation of the entire system reveals that in order to obtain a particular noise level on the output, the sensor noise has to be one order of magnitude lower. This particular ratio is not predicted by the noise sensitivity function that comes out linear control theory and might be the results of the non linearity present in the real system.

The time response is also improved compared to open-loop condition, going from 50ms to 20ms for slow sliding speed. The results could be more dramatic

with a more powerful actuator, since the current dynamic is only limited by the maximum amplitude that the plate can achieve.

6 Conclusion

This article presents the simulation and implementation of a surface-haptic device that is able to render precise and accurate stimuli to the sliding finger in a dynamic range of 0.3 to 0.9 N. In particular, we showed that the combination of force sensor with a wide dynamic range (1:50,000) and a PI controller was sufficient to considerably reduce the variability of the stimuli produced by ultrasonic friction modulation.

The performances of the current implementation are limited by the power of the ultrasonic plate and ongoing engineering will focus on building a more powerful actuator that can support quick and large variation of the amplitude. The online regulation of the friction force delivers frictional stimuli with high precision and accuracy and therefore this interface is a valuable tool for psychophysical experiments that require fine control over stimulus provided. The increase sharpness and fidelity is also a key asset for providing unambiguous virtual environments on user interfaces.

Acknowledgments

References

1. Shultz, C.D., Peshkin, M.A., Colgate, J.E.: The application of tactile, audible, and ultrasonic forces to human fingertips using broadband electroadhesion. In: World Haptics Conference (WHC), 2017 IEEE, IEEE (2017) 119–124
2. Biet, M., Giraud, F., Lemaire-Semail, B.: Squeeze film effect for the design of an ultrasonic tactile plate. ieee transactions on ultrasonics, ferroelectrics, and frequency control **54**(12) (2007)
3. Winfield, L., Glassmire, J., Colgate, J.E., Peshkin, M.: T-pad: Tactile pattern display through variable friction reduction. In: EuroHaptics Conference, 2007 and Symposium on Haptic Interfaces for Virtual Environment and Teleoperator Systems. World Haptics 2007. Second Joint, IEEE (2007) 421–426
4. Minsky, M., Ming, O.y., Steele, O., Brooks Jr, F.P., Behensky, M.: Feeling and seeing: issues in force display. In: ACM SIGGRAPH Computer Graphics. Volume 24., ACM (1990) 235–241
5. Robles-De-La-Torre, G., Hayward, V.: Force can overcome object geometry in the perception of shape through active touch. Nature **412**(6845) (2001) 445–448

6. Sednaoui, T., Vezzoli, E., Dzidek, B., Lemaire-Semail, B., Chappaz, C., Adams, M.: Experimental evaluation of friction reduction in ultrasonic devices. In: World Haptics Conference (WHC), 2015 IEEE, IEEE (2015) 37–42
7. Monnoyer, J., Diaz, E., Bourdin, C., Wiertlewski, M.: Optimal skin impedance promotes perception of ultrasonic switches. In: World Haptics Conference (WHC), 2017 IEEE, IEEE (2017) 130–135
8. Tomlinson, S., Lewis, R., Carré, M.: The effect of normal force and roughness on friction in human finger contact. Wear **267**(5) (2009) 1311–1318
9. Pasumarty, S.M., Johnson, S.A., Watson, S.A., Adams, M.J.: Friction of the human finger pad: influence of moisture, occlusion and velocity. Tribology Letters **44**(2) (2011) 117
10. Meyer, D.J., Wiertlewski, M., Peshkin, M.A., Colgate, J.E.: Dynamics of ultrasonic and electrostatic friction modulation for rendering texture on haptic surfaces. In: Haptics Symposium (HAPTICS), 2014 IEEE, IEEE (2014) 63–67
11. Wiertlewski, M., Friesen, R.F., Colgate, J.E.: Partial squeeze film levitation modulates fingertip friction. Proceedings of the National Academy of Sciences **113**(33) (2016) 9210–9215
12. Vezzoli, E., Messaoud, W.B., Amberg, M., Giraud, F., Lemaire-Semail, B., Bueno, M.A.: Physical and perceptual independence of ultrasonic vibration and electrovibration for friction modulation. IEEE transactions on haptics **8**(2) (2015) 235–239
13. Smith, T.A., Gorlewicz, J.L.: Hue: A hybrid ultrasonic and electrostatic variable friction touchscreen. In: World Haptics Conference (WHC), 2017 IEEE, IEEE (2017) 635–640
14. Wiertlewski, M., Leonardis, D., Meyer, D.J., Peshkin, M.A., Colgate, J.E.: A high-fidelity surface-haptic device for texture rendering on bare finger. In: International Conference on Human Haptic Sensing and Touch Enabled Computer Applications, Springer (2014) 241–248
15. Vezzoli, E., Sednaoui, T., Amberg, M., Giraud, F., Lemaire-Semail, B.: Texture rendering strategies with a high fidelity-capacitive visual-haptic friction control device. In: International Conference on Human Haptic Sensing and Touch Enabled Computer Applications, Springer (2016) 251–260
16. Messaoud, W.B., Amberg, M., Lemaire-Semail, B., Giraud, F., Bueno, M.A.: High fidelity closed loop controlled friction in smarttac tactile stimulator. In: Power Electronics and Applications (EPE'15 ECCE-Europe), 2015 17th European Conference on, IEEE (2015) 1–9
17. Lotters, J.C., Olthuis, W., Veltink, P.H., Bergveld, P.: A sensitive differential capacitance to voltage converter for sensor applications. IEEE Transactions on Instrumentation and Measurement **48**(1) (1999) 89–96
18. Wiertlewski, M., Hudin, C., Hayward, V.: On the 1/f noise and non-integer harmonic decay of the interaction of a finger sliding on flat and sinusoidal surfaces. In: World Haptics Conference (WHC), IEEE (2011) 25–30